JACS
JOURNAL OF THE AMERICAN CHEMICAL SOCIETY
pubs.acs.org/JACS
Communication

Selectively Addressable Photogenerated Spin Qubit Pairs in DNA Hairpins

Jacob H. Olshansky, Jinyuan Zhang, Matthew D. Krzyaniak, Emmaline R. Lorenzo, and Michael R. Wasielewski*

Cite This: J. Am. Chem. Soc. 2020, 142, 3346−3350
Read Online
ACCESS | Metrics & More | Article Recommendations | Supporting Information

ABSTRACT: Photoinduced electron transfer can produce radical pairs having two quantum entangled electron spins that can act as spin qubits in quantum information applications. Manipulation of these spin qubits requires selective addressing of each spin using microwave pulses. In this work, photogenerated spin qubit pairs are prepared within chromophore-modified DNA hairpins with varying spin qubit distances, and are probed using transient EPR spectroscopy. By performing pulse-EPR measurements on the shortest hairpin, selective addressing of each spin qubit comprising the pair is demonstrated. Furthermore, these spin qubit pairs have coherence times of more than 4 μs, which provides a comfortable time window for performing complex spin manipulations for quantum information applications. The applicability of these DNA-based photogenerated two-qubit systems is discussed in the context of quantum gate operations, specifically the controlled-NOT gate.

Quantum information science (QIS) has drawn considerable attention for its potential to revolutionize computing, communication, sensing, and other technologies.[1,2] Nevertheless, the key materials systems that will lead this revolution remain undetermined.[3] Electron spins readily serve as quantum bits (qubits);[4−6] in particular, photogenerated entangled spin qubit (radical) pairs (SQPs) using organic molecules offer unique advantages.[7−18] Photogenerated SQPs are synthetically tailorable, exhibit long coherence times, and, most importantly, are produced in a pure initial quantum state, allowing them to fulfill a key requirement for physical qubits.[19] SQPs have been shown to carry out spin teleportation[20] and to implement quantum gate operations;[12,13,21−23] however, in both cases the ability to uniquely address the individual qubits is critical.

Spatially addressable qubits have been demonstrated using scanning probe techniques,[24,25] and electrochemically addressable molecule-based electron spin qubits have also been demonstrated using gold−thiolate complexes.[26] Magnetic field or frequency-based addressability holds great promise, as it can be implemented on ensembles of qubits using readily available electron paramagnetic resonance (EPR) techniques with microwave pulse sequences.[6] A straightforward way to achieve addressability in a molecular system is to use spin qubits that possess distinct *g*-values. This strategy is termed *g*-engineering and has been applied to spin qubits composed of organic radicals,[27] 4f ions,[28] and 3d metal cages.[29] In two of these examples, researchers demonstrated a proof-of-principle controlled-NOT (CNOT) quantum gate operation that relied on the built-in addressability.[27,28] However, these examples illustrate a well-known limitation in QIS applications;[30] they employ thermally populated spin qubits, in which the purity of the initial quantum state is controlled solely by using high magnetic fields and <5 K temperatures.[27] In the present work, we use photogenerated SQPs that are initialized in a pure singlet quantum state at moderate temperatures (85 K) and *g*-engineer the system to achieve addressability.

DNA is a promising platform for QIS applications owing to its synthetic tunability, well-understood chemistry, and robust preparation methodologies. Furthermore, spatial addressability can be achieved using microchip arrays of DNA.[31,32] Synthetic DNA hairpins modified with chromophores have been extensively studied for more than two decades and have been shown to support photogenerated hole transfer through the π-stacked purines to create long-lived radical ion pairs that can serve as SQP states.[33−36] More recently, these SQPs have been successfully detected and characterized by time-resolved EPR (TREPR) spectroscopy using a continuous wave microwave source.[23,37−41] Since DNA supports hole transfer, the photogenerated SQPs have comprised chromophore radical anions and purine radical cations, including naphthalenediimide (NDI), anthraquinone (Aq), and perylenediimide (PDI), which yield $NDI^{\bullet-}-A^{\bullet+}$,[38] $NDI^{\bullet-}-G^{\bullet+}$,[37,38] $PDI^{\bullet-}-G^{\bullet+}$,[23,39,40] and $Aq^{\bullet-}-G^{\bullet+}$[23,41] SQPs. Furthermore, we have recently shown that by employing the stilbenediether (Sd) terminal hole acceptor, we could produce a high enough SQP yield to perform pulse-EPR experiments on the photogenerated $NDI^{\bullet-}-Sd^{\bullet+}$ SQP.[37] However, in all these cases the *g*-values of the two constituent radicals are not spectrally distinguishable, thus precluding spectral addressability.

The tetrathiofulvalene (TTF) radical cation has a particularly large *g*-value along its long *y*-axis;[42] therefore, when

Received: December 12, 2019
Published: February 2, 2020

https://dx.doi.org/10.1021/jacs.9b13398
J. Am. Chem. Soc. 2020, 142, 3346−3350

$TTF^{\bullet+}$ is generated by photoexcitation as part of a SQP and probed by TREPR spectroscopy, spectrally distinct, $TTF^{\bullet+}$ specific, features are observed.[11,14−17] The DNA hairpin structures explored in this study are shown in Figure 1a,

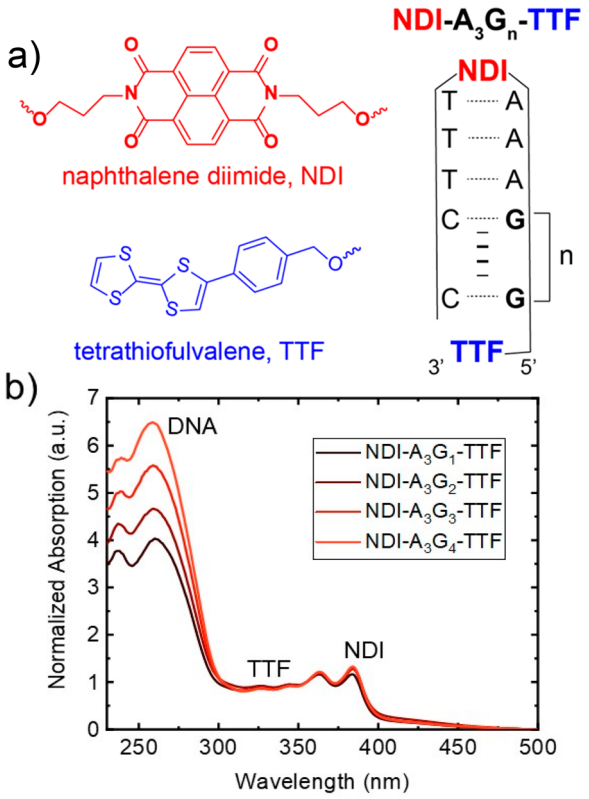

Figure 1. (a) DNA hairpins synthesized, n = 1−4. (b) Normalized UV−vis absorption spectra.

where an NDI hairpin linker and a three-adenine tract is followed by a variable length guanine tract (n = 1−4) and capped with the aryl TTF moiety. Photoexcitation of NDI results in hole transfer through the DNA to produce an $NDI^{\bullet-}$−$TTF^{\bullet+}$ SQP. We use TREPR and pulse-EPR spectroscopy to demonstrate that this SQP is not only prepared in a pure initial spin state at 85 K, but that the individual $NDI^{\bullet-}$ and $TTF^{\bullet+}$ spin qubits are selectively addressable by appropriately applied microwave pulses.

TTF has been incorporated into DNA previously using standard phosphoramidite chemistry.[43] The DNA hairpins in Figure 1a were synthesized using standard solid phase oligonucleotide synthetic techniques (see the Supporting Information (SI)). The UV−vis spectra (Figure 1b) show the presence of NDI and TTF in consistent ratios as well as an increasing concentration of DNA base pairs per molecule associated with longer hairpins. This observation confirms the synthesis of the intended structures with one NDI and TTF per hairpin.

Photoexcitation of NDI is followed by a series of exergonic hole transfer steps first to adenine then guanine and finally TTF, resulting in the $NDI^{\bullet-}$−$TTF^{\bullet+}$ SQP (Figure 2a). The dynamics of the initial charge separation processes are described elsewhere and influenced our choice of three-adenine diblock structures.[44,45] See SI for details. Our work with analogous NDI−A_3G_n−Sd hairpins suggests that we likely achieve SQP yields in the 10−20% range.[45] The $NDI^{\bullet-}$−$TTF^{\bullet+}$ SQPs charge recombine in 6 and 15 μs for hairpins with n = 1 and 2 respectively at 85 K (see SI).

TREPR and pulse-EPR measurements were performed on both Bruker Elexsys E680 X/W-band and lab-built pulse Q-band[20] spectrometers. Measurements were performed on DNA conjugates in 50% aqueous buffer and 50% glycerol at 85 K. Samples were photoexcited at 355 nm (see SI). The photogenerated $NDI^{\bullet-}$−$TTF^{\bullet+}$ SQPs were analyzed within the framework of the spin-correlated radical pair model.[7,8] Since the $NDI^{\bullet-}$−$TTF^{\bullet+}$ SQPs are produced from the ^{1}*NDI excited singlet state precursor, the initial spin state of these SQPs is a singlet state, $|S\rangle$. The spin−spin exchange interaction, $2J$, splits the singlet and triplet SQP state, while further splitting can occur in the solid state as a result of the spin−spin dipolar interaction, D. Applying a magnetic field, B_0, to the system results in Zeeman splitting of the triplet sublevels (Figure 2b). When $B_0 \gg J$ and D, the energies of the $|T_+\rangle$ and $|T_-\rangle$ states are substantially above and below that of $|T_0\rangle$ (m_s = 0), which is invariant to changes in B_0. Given that photogeneration of the SQP initially populates only $|S\rangle$, the difference in g-values and hyperfine interactions between the $NDI^{\bullet-}$ and $TTF^{\bullet+}$ mix $|S\rangle$ and $|T_0\rangle$ to produce two populated states, while $|T_+\rangle$ and $|T_-\rangle$ are unpopulated. Microwave-allowed transitions from the populated to the unpopulated states result in two absorptive and two emissive transitions (Figure 2c). The spin configurations in the uncoupled basis are shown next to the energy levels to highlight which spin flips are

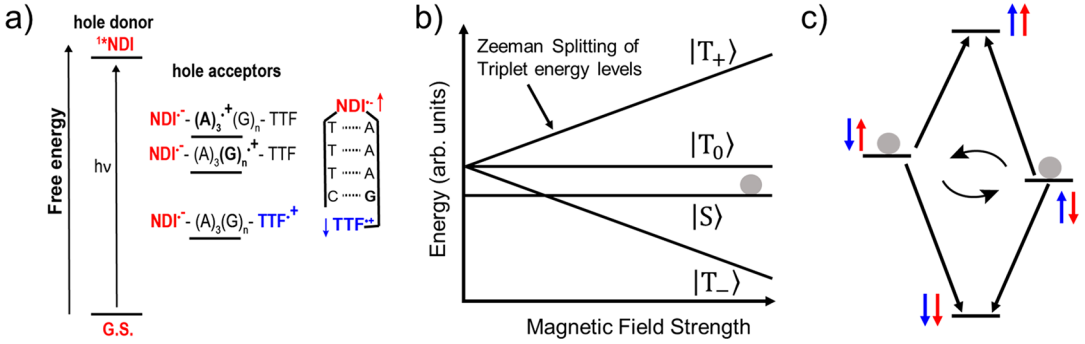

Figure 2. Electronic and spin state energies. (a) Relevant charge-separated species. The associated spins on NDI (red) and TTF (blue) are highlighted. (b) SQP in a magnetic field, showing selective population (gray circle) of the $|S\rangle$state. (c) SQP spin configurations shown in the uncoupled spin basis.

https://dx.doi.org/10.1021/jacs.9b13398
J. Am. Chem. Soc. 2020, 142, 3346−3350

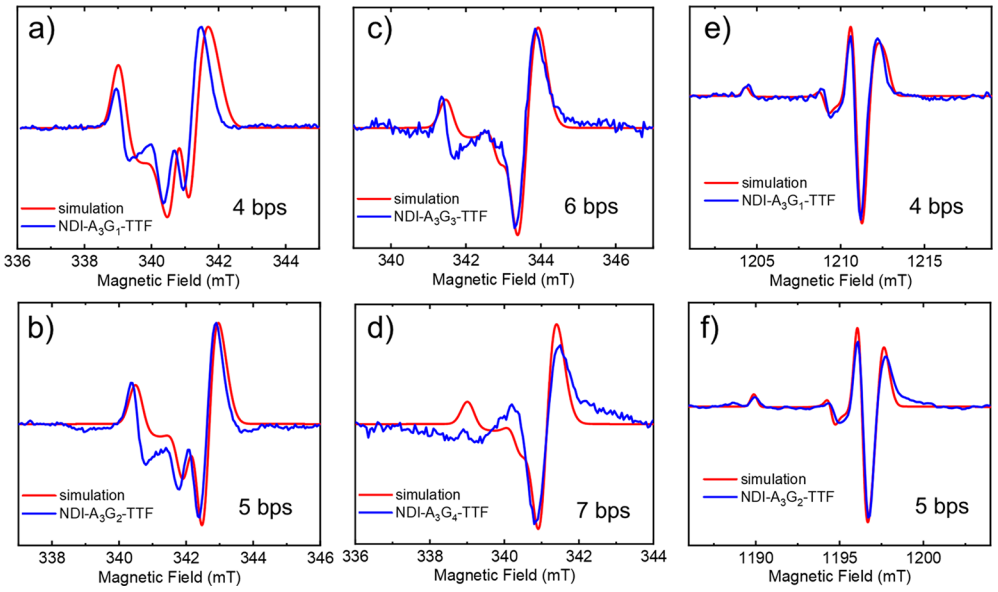

Figure 3. TREPR spectra of NDI−A_3G_n−TTF shown 100 ns after laser excitation. (a−d) X-band and (e,f) Q-band data (blue), simulations (red).

associated with each transition. In fact, these four states are the so-called Bell states of the 2-qubit spin system.[46]

TREPR spectra of $NDI^{\bullet-}$−$TTF^{\bullet+}$ in the DNA hairpins at both X-band and Q-band recorded 100 ns after laser excitation are shown in Figure 3. Given that the spectra are recorded using direct detection, positive signals are absorptive and negative signals are emissive. Simulations of the SQPs performed in Easyspin[47] are also shown. Each spectrum is composed of two absorptive and two emissive transitions (Figure 2c) that are derived from the *g*-values of the individual radicals and are offset from each other by an amount dependent on *J* and *D*.[48] The presence of these four transitions is not clear from the summed spectra in Figure 3 due to marked *g*-anisotropy that results in broadened transitions, especially from $TTF^{\bullet+}$ (see SI and Figure 4a for simulations decomposed into four components). In all spectra, the feature at low fields can be attributed to g_y associated with the long axis of the TTF molecule because it is significantly larger than all other *g*-value components in the $NDI^{\bullet-}$−$TTF^{\bullet+}$ SQP (see SI for calculations of all *g*-values).

A clear length dependence, resulting from the $1/r^3$ distance dependence of *D*, is observed in the X-band data (Figure 3a−d). Specifically, there is an emissive feature in the center of the spectra that is most pronounced for the shortest hairpin, smaller in the five base-pair hairpin, and not present in the longer hairpins. This feature was adequately captured by simulations that modulated *D* as a function of SQP separation in accordance with $1/r^3$. As we have observed before, short SQP separations (e.g., four base-pairs) result in *D* values that are on the order of the line width of the spectra and, therefore, cause line shape distortions, while longer hairpins lack these distortions.[37] Other parameters varied in the simulations included *J*, which was assumed to be near zero for all but the four base-pair sample, and the initial $|T_0\rangle$ population in the SQP. This initial $|T_0\rangle$ population can arise from singlet−triplet mixing in the initial $NDI^{\bullet-}$−purine$^{\bullet+}$ SQP states and ranged from 20% to 30% in our simulations. See the SI for the full fitting parameters. It should be noted that the seven base-pair sample (Figure 3d) has a very weak $TTF^{\bullet+}$ signal, indicating that the rate of hole transfer to TTF may not compete with that of charge recombination of $NDI^{\bullet-}$−$G^{\bullet+}$ in the longer hairpins. The broad background signal, not captured by simulation, may in fact be signal from this $NDI^{\bullet-}$−$G^{\bullet+}$ radical pair.

The data obtained at Q-band (higher B_0) for the two shortest hairpins illustrate the possibility for qubit addressability (Figure 3e−f). The simulations at Q-band were significantly less sensitive to the *J* and *D* parameters (due to the larger B_0), resulting in no perceptible difference between the two spectra. The effect of the initial $|T_0\rangle$ population and TTF orientation were systematically investigated (see SI) and confirm an initial $|T_0\rangle$ population of 20−30% and that the TTF is oriented parallel to NDI, as one would expect from a π-stacked hairpin geometry. The NDI−A_3G_1−TTF Q-band data are shown again in Figure 4a along with the simulation now decomposed into the four constituent transitions, two associated with $NDI^{\bullet-}$ (red) and two associated with $TTF^{\bullet+}$ (blue). These simulations show that the peak at the lowest

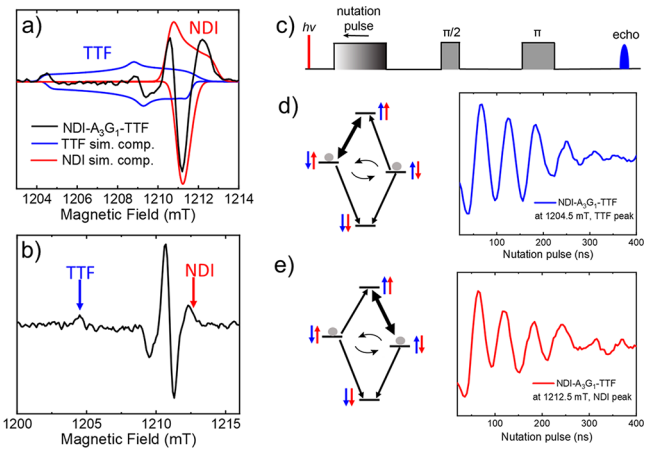

Figure 4. (a) TREPR data at Q-band with simulations decomposed into the four SQP transitions (see SI for properly scaled spectra). (b) Field-swept, echo-detected spectra for NDI-A_3G_1-TTF at Q-band. (c) Pulse sequence for nutation experiments. Rabi oscillations of the (d) TTF and (e) NDI transitions, highlighted in the SQP diagrams.

https://dx.doi.org/10.1021/jacs.9b13398
J. Am. Chem. Soc. 2020, 142, 3346−3350

field can be assigned solely to the $TTF^{\bullet+}$ absorptive transition, while the shoulder of the highest field transition is assigned to the $NDI^{\bullet-}$ absorptive transition. We used pulse-EPR to probe these individual transitions.

The field-swept echo data are shown in Figure 4b, indicating that these unique $TTF^{\bullet+}$ and $NDI^{\bullet-}$ transitions can be detected with pulse-EPR. We performed selective transient nutation experiments at the $TTF^{\bullet+}$ and $NDI^{\bullet-}$ absorptive transitions, demonstrating that we can selectively address these spin qubits. The transient nutation experiment allows for spin manipulation prior to the two-pulse echo detection scheme. Specifically, varying the length of the nutation pulse causes Rabi oscillations that can be read out in the echo amplitude. Nutation experiment results for the $TTF^{\bullet+}$ and $NDI^{\bullet-}$ absorptive transitions are shown in Figure 4d and 4e, respectively. The phase memory time (T_m) of this SQP was also determined to be approximately 2.7 μs in water/glycerol irrespective of hairpin length or whether NDI or TTF is probed, and greater than 4.0 μs in deuterated buffer (see SI). This corresponds to the coherence time for the entangled SQP and indicates that there is ample time to perform more complex microwave pulse-based spin manipulations.

A benchmark operation in multiqubit systems for QIS is the CNOT gate because this 2-qubit gate along with a suite of one qubit gates forms a complete set of gates necessary for quantum computation.[19] Microwave pulse sequences can implement a CNOT gate in an SQP system, as long as the spins are selectively addressable.[22,27] The experiments presented here along with our previous work[49] suggest that a DNA-based, photogenerated SQP could execute an unconditional CNOT gate, as well as providing a platform to prepare more complex multiqubit systems capable of quantum gate operations.

■ ASSOCIATED CONTENT

Supporting Information

The Supporting Information is available free of charge at https://pubs.acs.org/doi/10.1021/jacs.9b13398.

Synthesis and characterization, redox data, detailed sample preparation procedures, and additional EPR data and simulations (PDF)

■ AUTHOR INFORMATION

Corresponding Author

Michael R. Wasielewski − *Department of Chemistry and Institute for Sustainability and Energy at Northwestern, Northwestern University, Evanston, Illinois 60208-3113, United States;* orcid.org/0000-0003-2920-5440; Email: m-wasielewski@northwestern.edu

Authors

Jacob H. Olshansky − *Department of Chemistry and Institute for Sustainability and Energy at Northwestern, Northwestern University, Evanston, Illinois 60208-3113, United States;* orcid.org/0000-0003-3658-1487

Jinyuan Zhang − *Department of Chemistry and Institute for Sustainability and Energy at Northwestern, Northwestern University, Evanston, Illinois 60208-3113, United States*

Matthew D. Krzyaniak − *Department of Chemistry and Institute for Sustainability and Energy at Northwestern, Northwestern University, Evanston, Illinois 60208-3113, United States;* orcid.org/0000-0002-8761-7323

Emmaline R. Lorenzo − *Department of Chemistry and Institute for Sustainability and Energy at Northwestern, Northwestern University, Evanston, Illinois 60208-3113, United States*

Complete contact information is available at: https://pubs.acs.org/10.1021/jacs.9b13398

Notes

The authors declare no competing financial interest.

■ ACKNOWLEDGMENTS

This work was supported by the National Science Foundation under Grant No. CHE-1900422. E.R.L. was supported by a National Science Foundation Graduate Research Fellowship (DGE-1842165).

■ REFERENCES

(1) Biamonte, J.; Wittek, P.; Pancotti, N.; Rebentrost, P.; Wiebe, N.; Lloyd, S. Quantum machine learning. *Nature* **2017**, *549*, 195.

(2) Harrow, A. W.; Montanaro, A. Quantum computational supremacy. *Nature* **2017**, *549*, 203.

(3) Popkin, G. Quest for qubits. *Science* **2016**, *354* (6316), 1090−1093.

(4) Zajac, D. M.; Sigillito, A. J.; Russ, M.; Borjans, F.; Taylor, J. M.; Burkard, G.; Petta, J. R. Resonantly driven CNOT gate for electron spins. *Science* **2018**, *359* (6374), 439−442.

(5) Tokura, Y.; van der Wiel, W. G.; Obata, T.; Tarucha, S. Coherent Single Electron Spin Control in a Slanting Zeeman Field. *Phys. Rev. Lett.* **2006**, *96* (4), 047202.

(6) Misra, S. K., Quantum Computing/Quantum Information Processing in View of Electron Magnetic/Electron Paramagnetic Resonance Technique/Spectroscopy. In *Electron Spin Resonance (ESR) Based Quantum Computing*; Takui, T., Berliner, L., Hanson, G., Eds.; Springer New York: New York, NY, 2016; pp 1−23.

(7) Closs, G. L.; Forbes, M. D. E.; Norris, J. R., Jr. Spin-polarized electron paramagnetic resonance spectra of radical pairs in micelles: observation of electron spin-spin interactions. *J. Phys. Chem.* **1987**, *91* (13), 3592−9.

(8) Buckley, C. D.; Hunter, D. A.; Hore, P. J.; McLauchlan, K. A. Electron spin resonance of spin-correlated radical pairs. *Chem. Phys. Lett.* **1987**, *135* (3), 307−312.

(9) Hasharoni, K.; Levanon, H.; Greenfield, S. R.; Gosztola, D. J.; Svec, W. A.; Wasielewski, M. R. Mimicry of the Radical Pair and Triplet States in Photosynthetic Reaction Centers with a Synthetic Model. *J. Am. Chem. Soc.* **1995**, *117* (30), 8055−8056.

(10) Carbonera, D.; Di Valentin, M.; Corvaja, C.; Agostini, G.; Giacometti, G.; Liddell, P. A.; Kuciauskas, D.; Moore, A. L.; Moore, T. A.; Gust, D. EPR Investigation of Photoinduced Radical Pair Formation and Decay to a Triplet State in a Carotene−Porphyrin−Fullerene Triad. *J. Am. Chem. Soc.* **1998**, *120* (18), 4398−4405.

(11) Di Valentin, M.; Bisol, A.; Agostini, G.; Liddell, P. A.; Kodis, G.; Moore, A. L.; Moore, T. A.; Gust, D.; Carbonera, D. Photoinduced Long-Lived Charge Separation in a Tetrathiafulvalene−Porphyrin−Fullerene Triad Detected by Time-Resolved Electron Paramagnetic Resonance. *J. Phys. Chem. B* **2005**, *109* (30), 14401−14409.

(12) Miura, T.; Wasielewski, M. R. Manipulating Photogenerated Radical Ion Pair Lifetimes in Wirelike Molecules Using Microwave Pulses: Molecular Spintronic Gates. *J. Am. Chem. Soc.* **2011**, *133* (9), 2844−2847.

(13) Kobr, L.; Gardner, D. M.; Smeigh, A. L.; Dyar, S. M.; Karlen, S. D.; Carmieli, R.; Wasielewski, M. R. Fast Photodriven Electron Spin Coherence Transfer: A Quantum Gate Based on a Spin Exchange J-Jump. *J. Am. Chem. Soc.* **2012**, *134* (30), 12430−12433.

(14) Poddutoori, P. K.; Zarrabi, N.; Moiseev, A. G.; Gumbau-Brisa, R.; Vassiliev, S.; van der Est, A. Long-Lived Charge Separation in Novel Axial Donor−Porphyrin−Acceptor Triads Based on Tetrathia-

fulvalene, Aluminum(III) Porphyrin and Naphthalenediimide. *Chem. - Eur. J.* **2013**, *19* (9), 3148−3161.
(15) Kandrashkin, Y. E.; Poddutoori, P. K.; van der Est, A. Electron Transfer Pathways in a Tetrathiafulvalene-Aluminum(III) Porphyrin-Free-Base Porphyrin Triad Studied Using Electron Spin Polarization. *Appl. Magn. Reson.* **2016**, *47* (5), 511−526.
(16) Nelson, J. N.; Krzyaniak, M. D.; Horwitz, N. E.; Rugg, B. K.; Phelan, B. T.; Wasielewski, M. R. Zero Quantum Coherence in a Series of Covalent Spin-Correlated Radical Pairs. *J. Phys. Chem. A* **2017**, *121* (11), 2241−2252.
(17) Nelson, J. N.; Zhang, J.; Zhou, J.; Rugg, B. K.; Krzyaniak, M. D.; Wasielewski, M. R. Effect of Electron−Nuclear Hyperfine Interactions on Multiple-Quantum Coherences in Photogenerated Covalent Radical (Qubit) Pairs. *J. Phys. Chem. A* **2018**, *122* (49), 9392−9402.
(18) Wu, Y.; Zhou, J.; Nelson, J. N.; Young, R. M.; Krzyaniak, M. D.; Wasielewski, M. R. Covalent Radical Pairs as Spin Qubits: Influence of Rapid Electron Motion between Two Equivalent Sites on Spin Coherence. *J. Am. Chem. Soc.* **2018**, *140* (40), 13011−13021.
(19) DiVincenzo, D. P. The Physical Implementation of Quantum Computation. *Fortschr. Phys.* **2000**, *48* (9−11), 771−783.
(20) Rugg, B. K.; Krzyaniak, M. D.; Phelan, B. T.; Ratner, M. A.; Young, R. M.; Wasielewski, M. R. Photodriven quantum teleportation of an electron spin state in a covalent donor−acceptor−radical system. *Nat. Chem.* **2019**, *11* (11), 981−986.
(21) Filidou, V.; Simmons, S.; Karlen, S. D.; Giustino, F.; Anderson, H. L.; Morton, J. J. L. Ultrafast entangling gates between nuclear spins using photoexcited triplet states. *Nat. Phys.* **2012**, *8* (8), 596−600.
(22) Volkov, M. Y.; Salikhov, K. M. Pulse Protocols for Quantum Computing with Electron Spins as Qubits. *Appl. Magn. Reson.* **2011**, *41* (2), 145−154.
(23) Carmieli, R.; Thazhathveetil, A. K.; Lewis, F. D.; Wasielewski, M. R. Photoselective DNA Hairpin Spin Switches. *J. Am. Chem. Soc.* **2013**, *135* (30), 10970−10973.
(24) Baumann, S.; Paul, W.; Choi, T.; Lutz, C. P.; Ardavan, A.; Heinrich, A. J. Electron paramagnetic resonance of individual atoms on a surface. *Science* **2015**, *350* (6259), 417−420.
(25) Atzori, M.; Sessoli, R. The Second Quantum Revolution: Role and Challenges of Molecular Chemistry. *J. Am. Chem. Soc.* **2019**, *141* (29), 11339−11352.
(26) McGuire, J.; Miras, H. N.; Richards, E.; Sproules, S. Enabling single qubit addressability in a molecular semiconductor comprising gold-supported organic radicals. *Chem. Sci.* **2019**, *10* (5), 1483−1491.
(27) Nakazawa, S.; Nishida, S.; Ise, T.; Yoshino, T.; Mori, N.; Rahimi, R. D.; Sato, K.; Morita, Y.; Toyota, K.; Shiomi, D.; Kitagawa, M.; Hara, H.; Carl, P.; Hoefer, P.; Takui, T. A Synthetic Two-Spin Quantum Bit: g-Engineered Exchange-Coupled Biradical Designed for Controlled-NOT Gate Operations. *Angew. Chem., Int. Ed.* **2012**, *51* (39), 9860−9864.
(28) Aguilà, D.; Barrios, L. A.; Velasco, V.; Roubeau, O.; Repollés, A.; Alonso, P. J.; Sesé, J.; Teat, S. J.; Luis, F.; Aromí, G. Heterodimetallic [LnLn′] Lanthanide Complexes: Toward a Chemical Design of Two-Qubit Molecular Spin Quantum Gates. *J. Am. Chem. Soc.* **2014**, *136* (40), 14215−14222.
(29) Fernandez, A.; Moreno Pineda, E.; Muryn, C. A.; Sproules, S.; Moro, F.; Timco, G. A.; McInnes, E. J. L.; Winpenny, R. E. P. g-Engineering in Hybrid Rotaxanes To Create AB and AB2 Electron Spin Systems: EPR Spectroscopic Studies of Weak Interactions between Dissimilar Electron Spin Qubits. *Angew. Chem.* **2015**, *127* (37), 11008−11011.
(30) Warren, W. S. The Usefulness of NMR Quantum Computing. *Science* **1997**, *277* (5332), 1688−1690.
(31) Kruppa, P.; Frey, A.; Kuehne, I.; Schienle, M.; Persike, N.; Kratzmueller, T.; Hartwich, G.; Schmitt-Landsiedel, D. A digital CMOS-based 24 × 16 sensor array platform for fully automatic electrochemical DNA detection. *Biosens. Bioelectron.* **2010**, *26* (4), 1414−1419.
(32) Spehar-Délèze, A.-M.; Gransee, R.; Martinez-Montequin, S.; Bejarano-Nosas, D.; Dulay, S.; Julich, S.; Tomaso, H.; O'Sullivan, C. K. Electrochemiluminescence DNA sensor array for multiplex detection of biowarfare agents. *Anal. Bioanal. Chem.* **2015**, *407* (22), 6657−6667.
(33) Kawai, K.; Majima, T. Hole Transfer Kinetics of DNA. *Acc. Chem. Res.* **2013**, *46* (11), 2616−2625.
(34) Lewis, F. D.; Young, R. M.; Wasielewski, M. R. Tracking Photoinduced Charge Separation in DNA: from Start to Finish. *Acc. Chem. Res.* **2018**, *51* (8), 1746−1754.
(35) Lewis, F. D.; Kalgutkar, R. S.; Wu, Y.; Liu, X.; Liu, J.; Hayes, R. T.; Miller, S. E.; Wasielewski, M. R. Driving Force Dependence of Electron Transfer Dynamics in Synthetic DNA Hairpins. *J. Am. Chem. Soc.* **2000**, *122* (49), 12346−12351.
(36) Lewis, F. D.; Letsinger, R. L.; Wasielewski, M. R. Dynamics of Photoinduced Charge Transfer and Hole Transport in Synthetic DNA Hairpins. *Acc. Chem. Res.* **2001**, *34* (2), 159−170.
(37) Olshansky, J. H.; Krzyaniak, M. D.; Young, R. M.; Wasielewski, M. R. Photogenerated Spin-Entangled Qubit (Radical) Pairs in DNA Hairpins: Observation of Spin Delocalization and Coherence. *J. Am. Chem. Soc.* **2019**, *141* (5), 2152−2160.
(38) Nakajima, S.; Akiyama, K.; Kawai, K.; Takada, T.; Ikoma, T.; Majima, T.; Tero-Kubota, S. Spin-correlated radical pairs in synthetic hairpin DNA. *ChemPhysChem* **2007**, *8* (4), 507−509.
(39) Zeidan, T. A.; Carmieli, R.; Kelley, R. F.; Wilson, T. M.; Lewis, F. D.; Wasielewski, M. R. Charge-Transfer and Spin Dynamics in DNA Hairpin Conjugates with Perylenediimide as a Base-Pair Surrogate. *J. Am. Chem. Soc.* **2008**, *130* (42), 13945−13955.
(40) Carmieli, R.; Mi, Q.; Ricks, A. B.; Giacobbe, E. M.; Mickley, S. M.; Wasielewski, M. R. Direct Measurement of Photoinduced Charge Separation Distances in Donor-Acceptor Systems for Artificial Photosynthesis Using OOP-ESEEM. *J. Am. Chem. Soc.* **2009**, *131* (24), 8372−8373.
(41) Carmieli, R.; Smeigh, A. L.; Mickley Conron, S. M.; Thazhathveetil, A. K.; Fuki, M.; Kobori, Y.; Lewis, F. D.; Wasielewski, M. R. Structure and Dynamics of Photogenerated Triplet Radical Ion Pairs in DNA Hairpin Conjugates with Anthraquinone End Caps. *J. Am. Chem. Soc.* **2012**, *134* (27), 11251−11260.
(42) Hibbert, D. B.; Hamedelniel, A. E.; Sutcliffe, L. H. ESR and theoretical study of tetrathiofulvalene and dibenzotetrathiofulvalene and their radical cations. *Magn. Reson. Chem.* **1987**, *25* (7), 648−652.
(43) Bouquin, N.; Malinovskii, V. L.; Guégano, X.; Liu, S.-X.; Decurtins, S.; Häner, R. TTF-Modified DNA. *Chem. - Eur. J.* **2008**, *14* (19), 5732−5736.
(44) Renaud, N.; Harris, M. A.; Singh, A. P. N.; Berlin, Y. A.; Ratner, M. A.; Wasielewski, M. R.; Lewis, F. D.; Grozema, F. C. Deep-hole transfer leads to ultrafast charge migration in DNA hairpins. *Nat. Chem.* **2016**, *8* (11), 1015−1021.
(45) Olshansky, J. H.; Young, R. M.; Wasielewski, M. R. Charge Separation and Recombination Pathways in Diblock DNA Hairpins. *J. Phys. Chem. B* **2019**, *123* (7), 1545−1553.
(46) Bell, J. S. On the Einstein-Poldolsky-Rosen paradox. *Physics* **1964**, *1*, 195−200.
(47) Stoll, S.; Schweiger, A. EasySpin, a comprehensive software package for spectral simulation and analysis in EPR. *J. Magn. Reson.* **2006**, *178* (1), 42−55.
(48) Hore, P. J.; Hunter, D. A.; McKie, C. D.; Hoff, A. J. Electron paramagnetic resonance of spin-correlated radical pairs in photosynthetic reactions. *Chem. Phys. Lett.* **1987**, *137* (6), 495−500.
(49) Nelson, J. N.; Zhang, J.; Zhou, J.; Rugg, B. K.; Krzyaniak, M. D.; Wasielewski, M. R. CNOT gate operation on a photogenerated molecular electron spin-qubit pair. *J. Chem. Phys.* **2020**, *152* (1), 014503.

https://dx.doi.org/10.1021/jacs.9b13398
J. Am. Chem. Soc. 2020, 142, 3346−3350